

MIT Open Access Articles

An integrated model for quantifying the impacts of pavement albedo and urban morphology on building energy demand

The MIT Faculty has made this article openly available. **Please share** how this access benefits you. Your story matters.

As Published: 10.1016/J.ENBUILD.2020.109759

Publisher: Elsevier BV

Persistent URL: <https://hdl.handle.net/1721.1/136313>

Version: Author's final manuscript: final author's manuscript post peer review, without publisher's formatting or copy editing

Terms of use: Creative Commons Attribution-NonCommercial-NoDerivs License



An integrated model for quantifying the impacts of pavement albedo and urban morphology on building energy demand

Xin Xu^a, Hessam Azarijafari^{a}, Jeremy Gregory^a, Leslie Norford^b, Randolph Kirchain^c*

^a Department of Civil & Environmental Engineering, Massachusetts Institute of Technology,
Cambridge, MA 02139

^b Department of Architecture, Massachusetts Institute of Technology, Building 5-418D,
Cambridge, MA 02139

^c Materials Research Laboratory, Massachusetts Institute of Technology, Building E19-695,
Cambridge, MA 02139

* Corresponding author

Tel: 617-253-6467

Email: hessam@mit.edu

1 **ABSTRACT**

2 This contribution details a high-resolution approach to estimate the net greenhouse gas (GHG)
3 impact of changing pavement albedo in urban areas by accounting for both changes in air
4 temperature and building energy demand (BED) caused by the albedo change. The approach uses
5 machine-learning-based meta-models that allow stakeholders to estimate the impact of pavement
6 albedo modification for specific, detailed neighborhoods in a rapid, computationally efficient
7 manner. This method is applied to a case study involving all buildings and the adjacent pavements
8 in Boston, MA. Results from the case study indicate that increasing pavement albedo reduces
9 average temperature and usually reduces carbon emissions from BED for densely-built and
10 medium-density neighborhoods while results from low-density neighborhoods were mixed. Model
11 results suggest that increasing pavement albedo would lead to BED GHG benefits in 88% of
12 Boston neighborhoods. Increasing the albedo of the 1,100 miles of roads in those communities
13 would yield nearly 91,720 metric tons of reduced carbon emissions over the next fifty years.

14

15 *Keywords:* pavement albedo, building energy demand, urban morphology

16

17 **1 INTRODUCTION**

18 Urban surfaces, including roofs and pavements, play an important role in shaping the urban
19 microclimate, altering its energy balance and contributing to the so-called urban heat island (UHI)
20 effect [1]. UHIs have been associated with both increased energy demand from buildings and
21 deleterious health outcomes [2]. As global average temperatures rise, the magnitude of these
22 effects is only expected to grow. To address these concerns, public and private stakeholders have
23 begun to implement mitigation strategies. Ideally, each UHI mitigation strategy would not reduce
24 urban warming by creating other types of environmental burdens; if it did, decision-makers should
25 have quantitative information about the tradeoffs they would make.

26 Much has been written about the net environmental benefit for the most commonly cited mitigation
27 strategies including both “cool” roofs and additional greenspace [3-5]. One mitigation strategy that
28 has not been extensively studied is “cool” pavements. Cool pavements alter the energy balance of
29 the surrounding environment, typically through surface characteristics that reflect more solar
30 energy. This characteristic is referred to as albedo, with higher values representing higher
31 reflectance. Generally, there are two categories of climate-related effects related to pavement
32 albedo [6]. The first is a direct radiative forcing (RF) that results from the reflectance of energy
33 from the surface and back out of the atmosphere. The second effect is the change in energy demand
34 from nearby buildings (subsequently referred to as building energy demand or BED) and the
35 associated greenhouse gas (GHG) emissions from energy generation. We aim to fill a key gap in
36 understanding this second effect of cool pavements. Specifically, we explore how the impact of

37 cool pavements changes with urban form (i.e., morphology), using both a coupled physical-
38 simulation model and a novel, machine-learning model developed from thousands of physical
39 simulations. We then explore the net BED effects in the context of a case study of Boston,
40 Massachusetts. Results from the case study suggest that increasing pavement albedo usually
41 reduces carbon emissions from BED for densely-built and medium-density neighborhoods while
42 results from low-density neighborhoods were mixed. Model results suggest that increasing the
43 albedo would lead to BED GHG benefits in 88% of Boston neighborhoods. Increasing the albedo
44 of the 1,770 km of roads in those communities would yield more than 90,000 metric tons of
45 reduced carbon emissions over the next fifty years.

46 Recent research trends in building energy consumption entail models that consider a building in
47 the context of surrounding buildings in a neighborhood [7]. These models have been effective for
48 evaluating different building-level energy efficiency strategies. For large-scale energy modeling,
49 on the other hand, urban energy balance models such as urban canopy models (UCM) have been
50 widely adopted in the meteorological community. To reduce the computational cost, these models
51 usually consider the simplest neighborhood context. Usually UCMs represent an urban region as
52 a 1-D or 2-D canopy consisting of a single building and canyon floor, which is an oversimplified
53 representation of urban morphology [8]. In reality, the components of the outdoor environment
54 (buildings, streets, vegetation, etc.) have complex interactions with each other.

55 As computational power has become less costly, several research efforts have modeled the
56 interactions between buildings and the surrounding environment, accounting for the outdoor
57 energy balance and the indoor-outdoor energy exchanges [9-14]. Most of the modeling
58 frameworks require a co-simulation environment between building energy simulation engines and
59 urban-scale simulation engines, which capture effects at multiple scales. The earliest example of
60 this type of modeling is from Kikegawa et al. who coupled a one-dimensional urban canopy
61 meteorological model with a simple sub-model for building energy analysis [9]. Salamanca et al.
62 developed a building energy model (BEM) within an urban canopy parameterization for mesoscale
63 models [11]. Mauree et al. recently coupled the Canopy Interface Model (CIM) with CitySim, an
64 urban energy modeling tool to simulate the energy performance of buildings with different urban
65 forms and local climate [14]. While these coupled models were successfully implemented and
66 validated against measured data, they were limited to a few variations of urban form and context
67 within the investigated cities. Therefore, it's difficult to generalize the results to other contexts.
68 One exception is Quan et al. who conducted a parametric study of the density-energy relationship
69 to explore how building density, building shape, and building typology jointly influence building
70 energy performance. This work demonstrates the importance of urban morphology to energy
71 questions but did not explore its impact on urban microclimate or the impact of surface
72 characteristics [15].

73 Several studies have explored the climate implications of large-scale albedo modification related
74 to agriculture [16–19]. We are aware of only two studies that have addressed the specific issue of

75 how ground surface energy balance would affect BED. Yaghoobian et al. found a cooling load
76 savings of 17% in buildings due to a reduction in shortwave radiation transfer from the ground to
77 nearby buildings by using low-albedo ground surfaces [20]. In a later study, they found that
78 increasing pavement albedo from 0.1 to 0.5 near a four-story office building in Phoenix would
79 increase annual cooling loads up to 11% (33.1 kWh/m²), while the annual heating load was not
80 sensitive to such a modification [21]. Li et al. reported that the cooling effect of pavements has a
81 positive correlation with the peak value of solar radiation intensity [22]. In another study, Vox et
82 al. showed that the albedo of higher than 0.22 can result in a significant reduction of the surface
83 temperature mainly in the warmest hours [23]. During the night-time hours, no change in the
84 temperature was observed. These results indicate the potential of reflective pavements to have
85 significant impacts on adjacent buildings. Haley et al. used results from a regional climate
86 simulation and the EnergyPlus building energy simulation program [24] to assess the energy and
87 environmental consequences of cool pavements in Los Angeles and Fresno, California. Their work
88 also reinforces the fact that the net effect of increased incident radiation and reduced ambient
89 temperature on building energy due to pavement albedo increase is not intuitive [25].

90 These studies were critical in identifying the potential implications of surface albedo change.
91 However, because the required coupled physical simulation models are time-consuming to set up
92 and run, they have only been applied to a few urban forms. It would be valuable to better
93 understand the role of urban form on the implications of albedo change and to be able to rapidly

94 scan an urban area to identify neighborhoods where albedo change is likely to bring benefit. The
95 most promising areas can be studied in more detail.

96 In order to begin to fill that gap and guide future urban planning or design decisions, this study
97 investigates the impact of pavement albedo modification strategies on effective GHG emissions
98 and how that impact changes with urban form or morphology, as it is more formally known. The
99 hope is that this provides a more comprehensive picture of the role of pavement albedo
100 modification in the urban planner's toolkit.

101 **2 METHODOLOGY**

102 Albedo is defined as the proportion of reflected shortwave radiation (wavelength from 0.2 μ m-
103 3.0 μ m) to the total incoming shortwave radiation at the top of the atmosphere. In this study, we
104 considered the weighted mean value of albedo in an urban neighborhood (network level). To
105 address the limitations of existing building modeling frameworks, we developed machine-
106 learning-based meta-models that allow stakeholders to estimate the impact of pavement albedo
107 modification for specific, detailed neighborhoods in a rapid, computationally efficient manner.
108 The meta-models were developed from a large synthetic dataset of analyses executed in coupled-
109 physics models of energy exchange and use within a neighborhood. A hybrid modeling framework
110 was developed to create those analyses. This hybrid model combines the capabilities of several
111 existing tools, including the geometry generation tools Rhinoceros[®] (Rhino) and Grasshopper[®]
112 [26], the energy and radiation simulation plugin for Grasshopper[®], Ladybug and Honeybee [27],

113 and the urban climate simulator, Urban Weather Generator (UWG) [28]. The validation and
114 accuracy of these models have been studied by several researchers and have been validated
115 individually. Nevertheless, there is an opportunity for further studies to evaluate the uncertainty
116 related to using these tools together. Because the models are computationally expensive and
117 because urban morphology ranges over a broad multidimensional space, a parametric design of
118 experiments (DOE) was developed to efficiently map the impacts of urban morphology. The
119 workflow shown in Figure 1 can be summarized in four steps.

120 First, key urban morphological parameters were selected that influence building energy
121 consumption and a range of urban geometries, each with different combinations of morphological
122 parameters, were created using Rhino and Grasshopper [26]. The second step simulated the energy
123 flows and use in each neighborhood instance using the Urban Weather Generator (UWG) [28],
124 Ladybug, and Honeybee models. These two steps generated a synthetic dataset comprising the
125 morphological parameters for each neighborhood instance and four modeled temperature and
126 energy responses ΔT , ΔE^C , ΔE^H , and $\Delta E = \Delta E^C + \Delta E^H$ that represent temperature, cooling
127 heating BED and total BED change, respectively. It should be noted that both cooling and heating
128 changes are estimated based on their thermal energy values. Third, using this dataset, statistical
129 meta-models were developed to relate responses to the descriptive parameters. Finally, in order to
130 demonstrate the methodology in a realistic urban setting, detailed information related to the
131 morphology of real neighborhoods was extracted from a geographic information system (GIS)
132 database at the building level. The meta-models were then applied to predict changes in BED for

133 every building considering realistic urban context, based on the extracted morphological
 134 parameters. The next sections explain an overview of each of these steps.

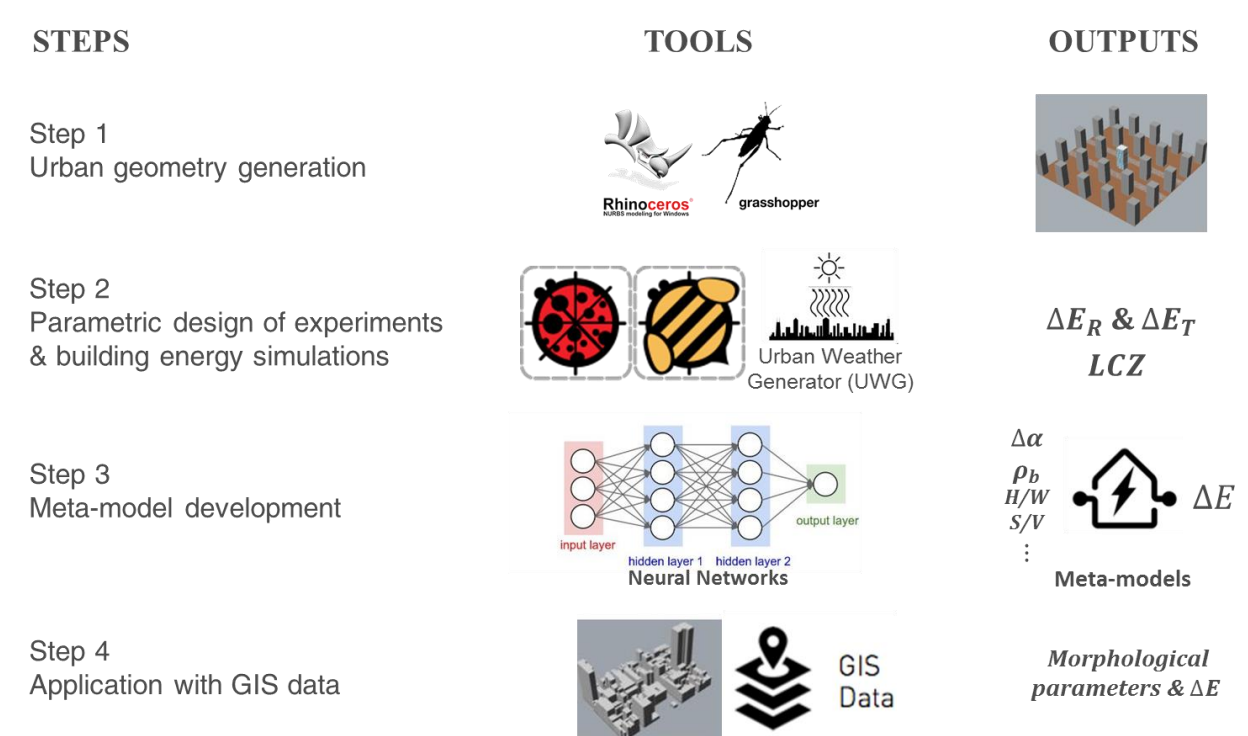


Figure 1. Modeling framework for studying the impact of pavement albedo ($\Delta\alpha$ is pavement albedo change; ΔE_R is the change in BED due to incident radiation; ΔE_T is the change in BED due to ambient temperature)

135

136 2.1 Urban Geometry Generation

137 Generating various urban geometries and assigning each building to one of the defined geometries
 138 enable one to capture the details of neighborhood characteristics. In addition, the generated
 139 geometries provide references for the meta-models to facilitate the BED change estimation of
 140 individual buildings in a rapid and computationally efficient way. Hence, this step should be

141 conducted in a careful manner to take into account the important morphology parameters that can
142 influence the BED response to the albedo change.

143 2.1.1 Selection of urban morphological parameters

144 A list of morphological parameters that may influence energy use and heat island effects was
145 extracted from the literature and presented in the Supporting Information (SII). Based on initial
146 single-variable sensitivity analyses, we identified four key morphological parameters that
147 significantly influence the impact of pavement albedo modification on BED: *building height* (H),
148 *canyon aspect ratio* (H/W), *building density* (ρ_b), and *building length* (L).

149 We organized and bounded our exploration of morphology based on a taxonomy developed by
150 Stewart & Oke [29]. To better understand the drivers of urban microclimate, Stewart & Oke
151 categorized neighborhoods into what they called local climate zones (LCZs) and identified ten
152 different urban and sub-urban LCZs. For each neighborhood characteristic (H , H/W , ρ_b and L), we
153 defined five evenly spaced levels to cover the ranges for each LCZ identified by Stewart & Oke
154 from empirical studies [29]. The specific values used in this study are shown in Table 1.

155 To construct a fully dimensionless meta-model, two dimensionless parameters, i.e., shape factor
156 (S/V) and façade density (ρ_f), were derived for each neighborhood geometry based on the four
157 known parameters. Shape factor was defined as the ratio of the surface area (S) to volume (V) for
158 a given building and was approximated as the ratio of the building's perimeter (r) to its footprint
159 area (fa). Formally, this is stated as:

160
$$\frac{S}{V} = \frac{S}{V} \approx \frac{r}{fa} \quad (1)$$

161 Façade density (ρ_f) was defined as the ratio of the street-facing surface area ($H \times L$) to the building
162 footprint area (fa).

163 These two parameters, plus the *canyon aspect ratio* (H/W) and *building density* (ρ_b), were then
164 used to build the meta-models. These were chosen as the model predictors because each impacts
165 pavement albedo-induced BED from different perspectives. Building density (ρ_b) and façade
166 density (ρ_f) directly determine the area of buildings and building walls affected by changes in the
167 amount of incident radiation received and reflected from the pavements. They also impact the
168 changes in canyon temperature. Canyon aspect ratio (H/W) affects the amount of solar radiation
169 incident on the canyon floor, as higher buildings and narrower canyons result in more shading and
170 less incident radiation. Finally, shape factor (S/V), defined as the surface area to volume ratio,
171 influences the effect of ambient temperature change on BED.

172 Because of the computational intensity of the models, we applied a fractional factorial design
173 method for an analysis comprising ten LCZs. We specifically used a design comprising 2,960
174 neighborhood configurations – about half of a full factorial design. To select this fraction, we
175 executed a full factorial analysis of one LCZ and found this fraction to lead to less than a 5%
176 decrease in model performance (as measured by R-squared). Changes in BED (ΔE) due to a 0.2
177 increase in pavement albedo ($\Delta\alpha = 0.2$) were simulated and recorded for each neighborhood

178 configuration in the experimental design. A change of 0.2 was modeled because this is a widely
179 used value for the difference in albedo between asphalt and concrete pavements and the potential
180 increase in pavement albedo due to the use of a reflective coating [30].

181 2.1.2 Urban geometry generation: Rhino with Grasshopper

182 Three-dimensional urban geometries used for this research were generated within Rhino, a CAD-
183 based modeling environment used by urban designers and architects [31]. Grasshopper is a plugin
184 for Rhino that allows algorithmic modeling and parametric simulations. Using Grasshopper, we
185 defined a parametric representation of a reference neighborhood that contains buildings with
186 identical structural and thermal characteristics and a street network in between. The building
187 dimensions and spacing, and therefore the scale of the neighborhood, were defined by the four
188 morphological parameters – shape factor (S/V), façade density (ρ_f), canyon aspect ratio (H/W),
189 and building density (ρ_b).

190 A key question concerning the definition of these reference neighborhoods is their size. The area
191 of the modeled neighborhood should not be so small that it is not representative of the urban fabric.
192 For the purposes of our study, a very small neighborhood would not allow for the possibility of
193 multiple reflections of radiation among buildings and street. At the same time, the reference
194 neighborhood should not be too large, because it increases computational expense. According to
195 Stewart & Oke [29], an LCZ typically spans from 400 meters to 1 kilometer in length of any side.

196 To align with this scale, our reference neighborhood comprised three blocks of buildings, each
 197 with two sets of five buildings, separated by two pavements in between, as shown in Figure 2. The
 198 building in the center of the middle row (indicated with a white roof, used only for emphasis in
 199 the figure; all buildings were modeled with the same roof characteristics) is the reference building
 200 (RB) for energy or radiation simulations. To support the DOE, 2,960 3D urban geometries were
 201 created.

202 *Table 1. Physical characteristics for the 10 local climate zones (Source: Stewart & Oke [29]).*

Local climate zone (LCZ)	Canyon aspect ratio	Building density	Average building height (m)	Sky view factor
<i>LCZ 1 Compact high-rise</i>	>2	0.4-0.6	>25	0.2-0.4
<i>LCZ 2 Compact mid-rise</i>	0.75-1.5	0.4-0.7	8-20	0.3-0.6
<i>LCZ 3 Compact low-rise</i>	0.75-1.5	0.4-0.7	3-8	0.2-0.6
<i>LCZ 4 Open high-rise</i>	0.75-1.25	0.2-0.4	>25	0.5-0.7
<i>LCZ 5 Open mid-rise</i>	0.3-0.75	0.2-0.4	8-20	0.5-0.8
<i>LCZ 6 Open low-rise</i>	0.3-0.75	0.2-0.4	3-8	0.6-0.9
<i>LCZ 7 Lightweight low-rise</i>	1-2	0.6-0.9	2-4	0.2-0.5
<i>LCZ 8 Large low-rise</i>	0.1-0.3	0.3-0.5	3-10	>0.7
<i>LCZ 9 Sparsely built</i>	0.1-0.25	0.1-0.2	3-8	>0.8
<i>LCZ 10 Heavy industry</i>	0.2-0.5	0.2-0.3	5-15	0.6-0.9

203

204

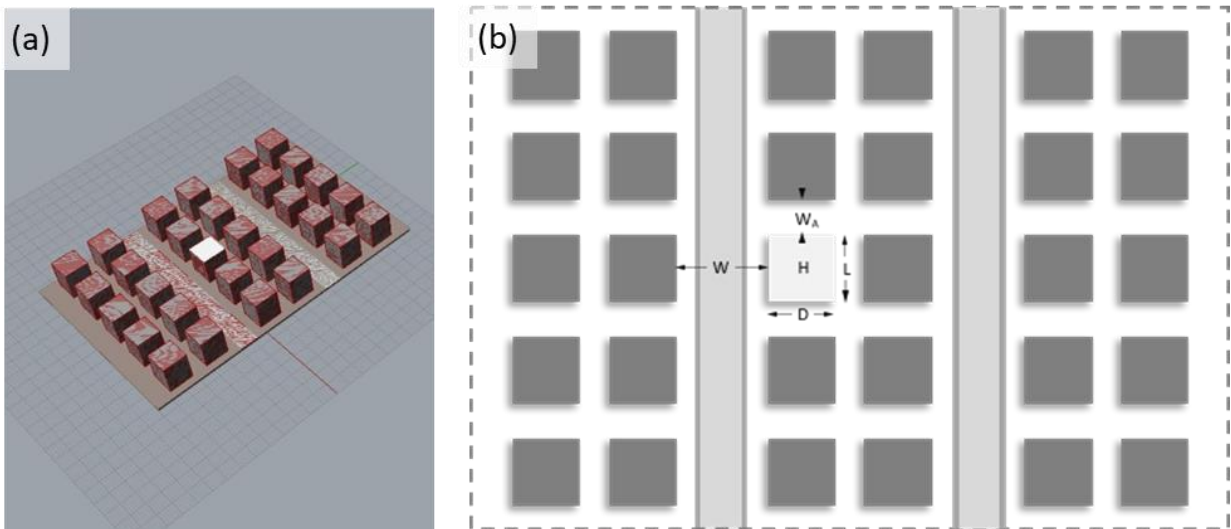


Figure 2. A generic urban neighborhood for the parametric analysis in the Rhinoceros interface. (a) perspective view; (b) top view. The building in the center of the middle row (indicated with white roof) is the reference building of interest for energy or radiation simulations. White is only used for emphasis. All buildings were modeled with the same roof characteristics.

205

206 2.2 Parametric Design of Experiments and Building Energy Simulations

207 Modifying the albedo of pavements has at least two effects that alter energy use in the reference
 208 building (RB): it alters the ambient temperature near the RB and the intensity of radiation incident
 209 on that building. To capture both of these effects, we made use of two modeling platforms that are
 210 described in more detail in the next two subsections. Here we give an overview of how their results
 211 were used to arrive at a final estimate of energy impact.

212 First, for the reference building in each neighborhood instance (i), we estimated the ambient
 213 temperatures when albedo is low (baseline temperature: $T_i|_{\alpha_{Low}} = T_{iL}$) and when albedo is high
 214 ($T_i|_{\alpha_{High}} = T_{iH}$). Second, we used a neighborhood energy simulation platform to model annual

215 energy use (E_i) for the RB. Formally, we evaluated heating (E_i^H) and cooling energy (E_i^C) use
216 separately.

217 Specifically, we used the neighborhood energy simulation to estimate the change in energy use,
218 ΔE_i , as the difference in energy use when albedo is high (α_H) and temperature is as expected for
219 high albedo, $E_{i,\alpha_H,T_{iH}}^H$ and $E_{i,\alpha_H,T_{iH}}^C$, and when albedo is low (α_L) temperature is baseline, $E_{i,\alpha_L,T_{iL}}^H$ and
220 $E_{i,\alpha_L,T_{iL}}^C$. For these analyses, both incident radiation and ambient temperature differ.
221 Mathematically, this is stated as

$$222 \quad \Delta E_i^\xi = \left(E_{i,\alpha_H,T_{iH}}^\xi - E_{i,\alpha_L,T_{iL}}^\xi \right) \quad (2)$$

223 where ξ is either H or C.

224 2.2.1 Radiation and building energy simulation with Ladybug & Honeybee

225 Ladybug and Honeybee (LaH) connect Grasshopper to several validated physics simulation
226 engines, such as EnergyPlus™, Radiance, DAYSIM, and OpenStudio® for building energy,
227 comfort, daylighting, and lighting simulation [27]. Using this tool, it is possible to simulate both
228 multiply-reflected transfers of shortwave radiation (using the Radiance engine) and building
229 energy consumption (using the EnergyPlus™ engine). EnergyPlus™ performs a full yearly
230 thermal dynamic simulation. As a result, annual energy consumption for heating (E_i^H) and cooling

231 (E_i^c) were modeled. The procedure of radiation and building energy simulation is detailed in the
232 Supporting Information section SI3.

233 2.2.2 Microclimate/ambient temperature simulation with UWG

234 UWG is an urban design simulation tool that provides climate-specific temperatures for cityscape
235 geometry and land-use change [32]. It estimates the hourly urban canyon air temperature and
236 humidity based on weather data from a rural weather station. The model takes as input the weather
237 file for a nearby rural weather station and parameters that describe urban morphology and surface
238 materials (this latter point makes it suitable for studying the impact of changing surface albedo).
239 The output from UWG is a modified weather file (.epw) that captures UHI effects and is
240 compatible with many building performance simulation programs, including EnergyPlus. The tool
241 has been tested for several urban areas and can satisfactorily estimate urban temperatures in
242 different climates, weather conditions, and urban configurations [28]; its performance is
243 comparable to a more computationally expensive mesoscale atmospheric model [33]. It should be
244 noted that meteorological parameters, such as global irradiances used in the weather file, were
245 implemented as input parameters in UWG for temperature simulation as well as Radiance for
246 daylight calculations. Details related to the weather file modification are presented in the
247 Supporting Information section SI4.

248 2.2.3 Simulations to develop synthetic dataset

249 The LaH and UWG models were executed for a set of 2,960 urban geometries assuming the
250 weather conditions for Boston, MA (case study described in a subsequent section). For each

251 simulation, the RB was assumed to meet ASHRAE standards 90.1-2010 [34] for climate zone 5A
252 as defined in LaH.

253 Previous studies have shown that the albedo of pavements changes as a function of time and use.
254 Generally, the albedo of new asphalt pavements increases and the albedo of new concrete
255 pavements declines. However, a robust model reflecting such dynamics has not been reported in
256 the literature [3,33]. In addition, a simulation of the time-dependent albedo for multiple cities
257 shows that the average albedo of the network may not change during a period of 50 years due to
258 periodic maintenance and repair of the pavement surface [36]. As such, in this study, we considered
259 albedo values that represent an average of aged and new pavements as reported in different studies
260 [37]. This is analogous to the approaches taken by Rosado and Levinson [38] and Guo et al. [39]
261 in evaluating changes in roof albedo and wall albedo, respectively. Hence, we estimate the impact
262 of albedo change by comparing the simulated result from a baseline scenario where albedo is low
263 ($\alpha_L=0.1$) with that from an increased-albedo scenario ($\alpha_H=0.3$).

264 2.3 Meta-models for predicting BED due to Pavement Albedo Modification

265 Using the results of the 2,960 simulations, meta-models with response variables of changes in
266 heating BED (ΔE_i^H) and cooling BED (ΔE_i^C) for the reference building in an LCZ were developed.
267 To identify the best model form, we evaluated various machine-learning models to fit the data,
268 including multiple regression, random forest regression, support vector machine, and neural
269 networks. For each LCZ, these model forms were tested and evaluated using 10-fold cross-
270 validation to avoid overfitting of the model. Neural networks were found to best predict ΔE due

271 to $\Delta\alpha$. The root mean square error (RMSE) and R-squared of the meta-models for the 10 LCZs in
272 the case of Boston (case study described in the next section) are summarized in the Supporting
273 Information section SI5.

274 2.4 Application to realistic neighborhoods with GIS data

275 GIS data is widely used in spatial analysis and urban planning to support decision-making. For the
276 case study developed here, shapefiles containing building information of Boston were obtained
277 from MassGIS (Bureau of Geographic Information) [40]. These shapefiles provide data on
278 building footprints, building heights, building types, etc. for 129,370 buildings in Boston. In
279 addition, vector data containing primary road networks for Boston was found in TIGER/Line®
280 shapefiles from the U.S. Census Bureau [41]. The procedure of applying the proposed method to
281 the Boston case study are presented in the Supporting Information section SI6.

282 2.4.1 Computing overall global warming potential results

283 Applying the meta-models, changes in BED (ΔE_i^H and ΔE_i^C) due to a 0.2 increase in pavement
284 albedo were estimated for every building described in the Boston shapefile. To estimate the impact
285 of increasing pavement albedo at a neighborhood scale or even at a city scale, the results for
286 individual buildings were then aggregated for each census tract. Whether at the building level or
287 for the census tract, the global warming potential (GWP) impact of increasing pavement albedo
288 was calculated from changes in cooling and heating BED, multiplied by the corresponding CO₂
289 emission factors for cooling and heating, respectively. The procedure for calculating the emission

290 factors for different environmental modeling scenarios is detailed in SI7 of the Supporting
291 Information.

292 **3 RESULTS AND DISCUSSION**

293 3.1 DOE results and discussion

294 Results from the DOE for Boston show that canyon aspect ratio (H/W), building density (ρ_b),
295 façade density (ρ_f), and surface-area-to-volume ratio (S/V) can all alter BED due to changes in
296 pavement albedo, but their influence on cooling demand and heating demand is different.

297 3.1.1 Influence of canyon aspect ratio (H/W), building density (ρ_b), and façade density (ρ_f)

298 Figure 3 plots the observed change in cooling and heating energy for various levels of H/W , ρ_b ,
299 and ρ_f for the DOE results of reference buildings in LCZ 2 neighborhoods. Because several
300 variables were changed for each neighborhood configuration within the experimental design,
301 significant scatter is observed in Figure 3. Nevertheless, some key trends are observable. Figure
302 3a shows that the change in cooling demand first increases slightly, but decreases quickly after
303 H/W approaches 1. When the aspect ratio is small (<0.94), the context resembles a wide canyon,
304 where buildings are far apart and/or the average building height is small. In this case, modifications
305 to pavements exert only a small impact on surrounding buildings. Nevertheless, as H/W grows,
306 one of two effects occurs: 1) H grows so that the cross-section of the building receiving incident
307 radiation grows, or 2) W shrinks so that incident radiation dissipates less before it impacts the
308 building (The change in delta incident radiation as a function of aspect ratio is presented in SI3).

309 In either case, ΔE_c first increases as H/W grows. However, as the canyon aspect ratio continues to
310 increase beyond around 1.0, the amount of shading from buildings to pavement or to other
311 buildings increases and ΔE_c begins to decline. As shown in Figure 3b, ΔE_h follows a somewhat
312 muted, inverse pattern – first becoming more negative then approaching zero as H/W increases.

313 Based on the results of this experimental design, the impact of ρ_b is less pronounced than that of
314 H/W . As shown in Figure 3c and d, ΔE_c due to pavement albedo change becomes slightly more
315 negative with ρ_b , while ΔE_h approaches zero as ρ_b increases. Figure 3e and f indicate that ΔE_h
316 changes more with changes to façade density (ρ_f) than does ΔE_c . Generally, ΔE_h becomes more
317 negative as ρ_f increases, while ΔE_c becomes slightly less negative as ρ_f increases.

318

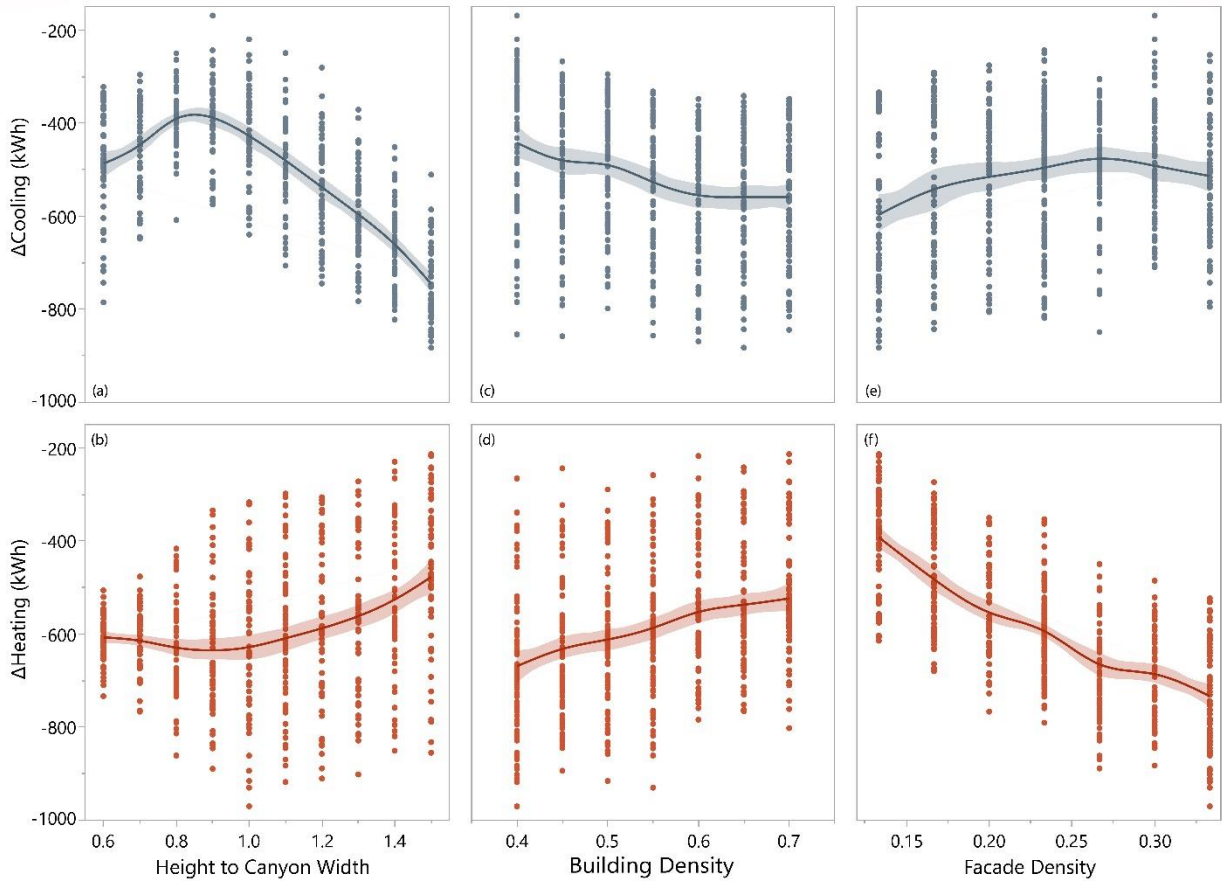


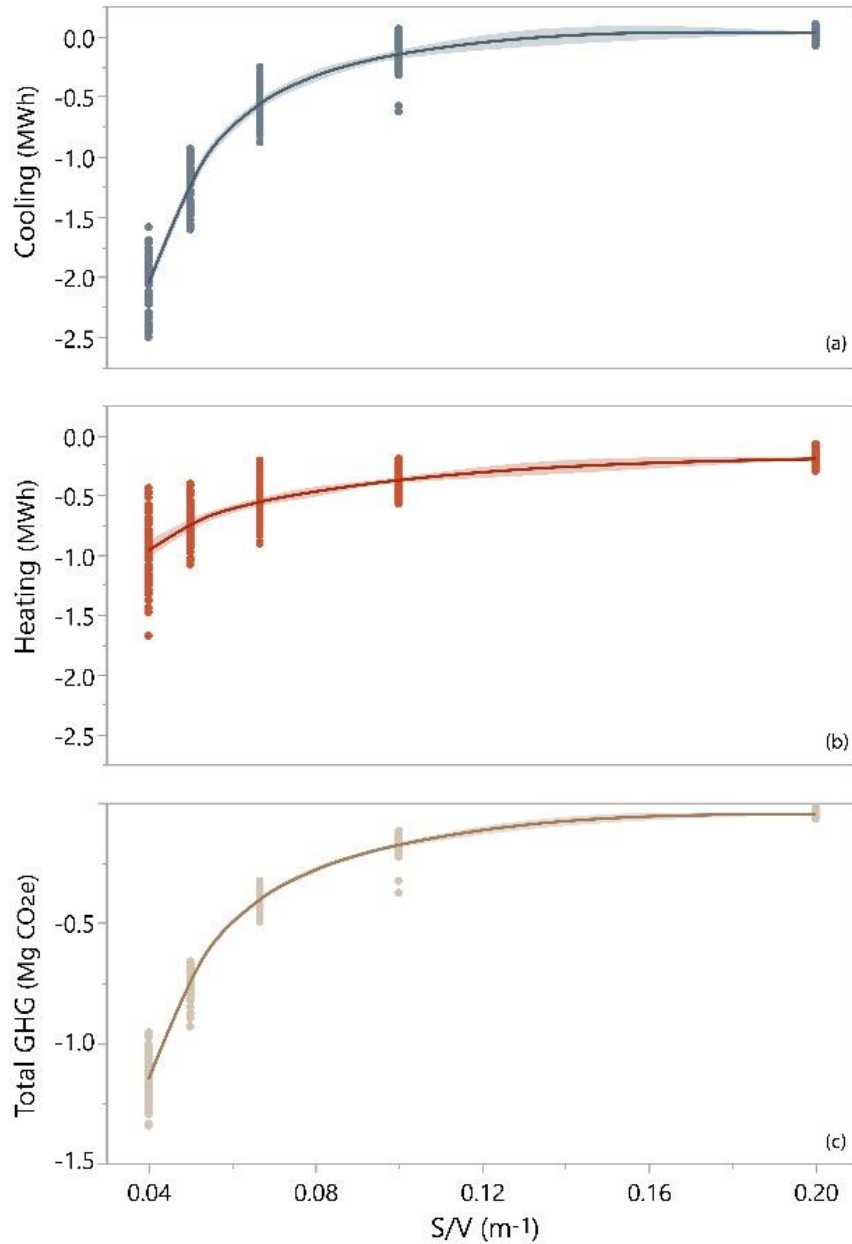
Figure 3. Changes in annual values of (thermal) cooling demand (a, c, and e) and (thermal) heating demand (b, d, and f) for Boston LCZ 2 due to 0.2 increase in pavement albedo for samples with different values of canyon aspect ratio (H/W) and building density (ρ_b) and façade density (ρ_f). Each point represents one neighborhood configuration modeled as part of the design of experiments. Lines represent the mean of observed responses. Shaded region represents a 95% confidence interval of mean.

319

320 3.1.2 Influence of shape factor (S/V)

321 Surface-to-volume ratio (S/V) is a measure of building compactness that is considered to play a
 322 significant role in building thermal exchanges [42]. Generally, for a constant building volume,
 323 increasing surface-to-volume ratio increases the energy demand in buildings. In this analysis, a

324 strong change in ΔE due to pavement albedo as S/V changes is evident. In fact, as shown in Figure
325 4, we observe that that for LCZ 2, change in cooling demand, change in heating demand and net
326 GHG all increase asymptotically as S/V increases. As a result, considering the net thermal changes,
327 the impact of changing pavement albedo is more significant for buildings with lower shape factors.



328

329 *Figure 4. Changes in cooling demand (a), heating demand (b), and total GHG emissions (c) for Boston*
330 *LCZ2 neighborhoods due to a 0.2 increase in pavement albedo for reference buildings with different*
331 *shape factors.*

332 3.1.3 Incident radiation vs. ambient temperature

333 It should be noted from Figure 3a that the changes in cooling BED due to increased pavement
334 albedo are slightly negative (cooling energy savings) when H/W is small. As H/W grows, energy-
335 saving first shrinks (becomes a smaller negative number) but then grows (becomes more negative)
336 as H/W grows or the neighborhood becomes denser. The switch in the direction of this trend reveals
337 a trade-off between the two mechanisms: incident radiation and ambient temperature, which can
338 be explained by the underlying physics. In EnergyPlus, energy demand is calculated by solving a
339 series of heat balance equations on building surfaces and on indoor air [43].

340 On the building external wall, the heat balance can be written as:

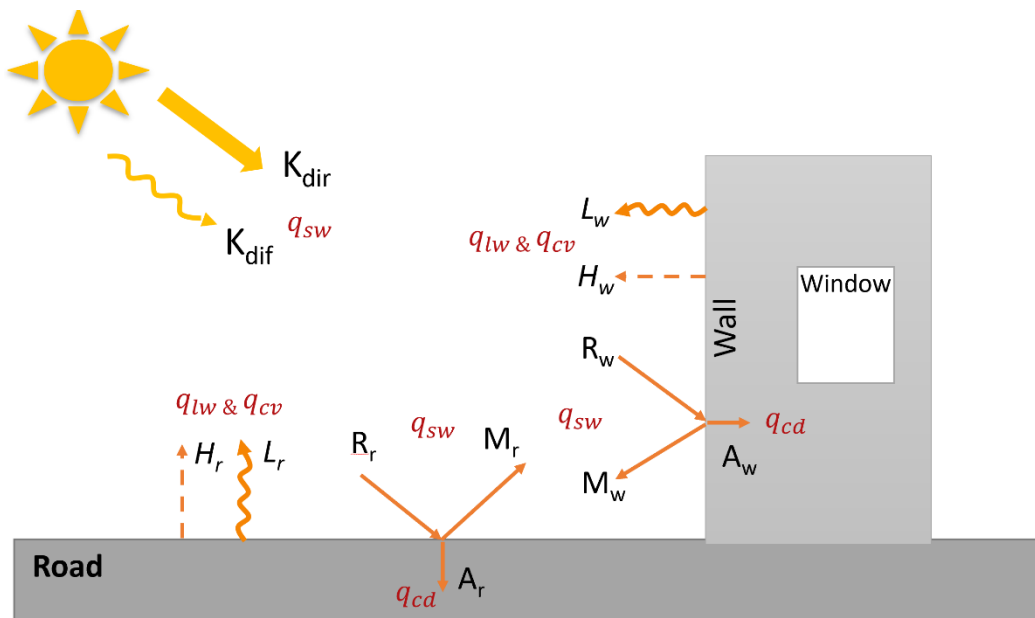
341
$$q_{sw} + q_{lw} + q_{cv} - q_{cd} = 0$$

342 where q_{sw} is the shortwave radiation, including direct, reflected and diffused solar radiation
343 q_{lw} is the longwave radiation from the environment, including sky, air, and the ground
344 q_{cv} is the convective flux from the environment
345 q_{cd} is the conductive flux through the wall
346

347 Increasing pavement albedo has a direct effect on q_{sw} ; more solar radiation is reflected from the
348 pavement. It also causes the ambient air temperature to reduce, as does the ground temperature.

349 As a result, both the longwave radiation q_{lw} and the convective flux q_{cv} from the environment
350 decrease. The net balance of the increased q_{sw} and decreased $(q_{lw} + q_{cv})$ determines the direction
351 of conductive flux q_{cd} through the wall, ultimately affecting the heat gain and energy demand
352 indoor. The relative magnitude of the shortwave q_{sw} and the longwave radiation q_{lw} depends on

353 urban morphology, which is why the slope change is observed for changes in cooling BED in
 354 Figure 3a. Figure 5 shows the schematic view of the heat balance on the building wall that faces
 355 the pavement. One should note that EnergyPlus does not automatically take into account the
 356 temperature changes at different altitudes and therefore, in this sense, the energy consumption on
 357 different floors is not captured. Further studies are required to add this feature to the BED
 358 simulation and a model evolved from the UWG, the Vertical City Weather Generator, estimates a
 359 vertical profile of ambient air temperature [44].



360

361 *Figure 5. schematic view of heat balance on the building wall exposed to the pavement side (H =*
 362 *convective heat transfer, L = longwave radiation, K_{dir} = direct radiation, K_{dif} = diffused radiation, R =*
 363 *incoming shortwave radiation M = Outgoing shortwave radiation, A = absorbed radiation, r = road, w =*
 364 *wall)*
 365

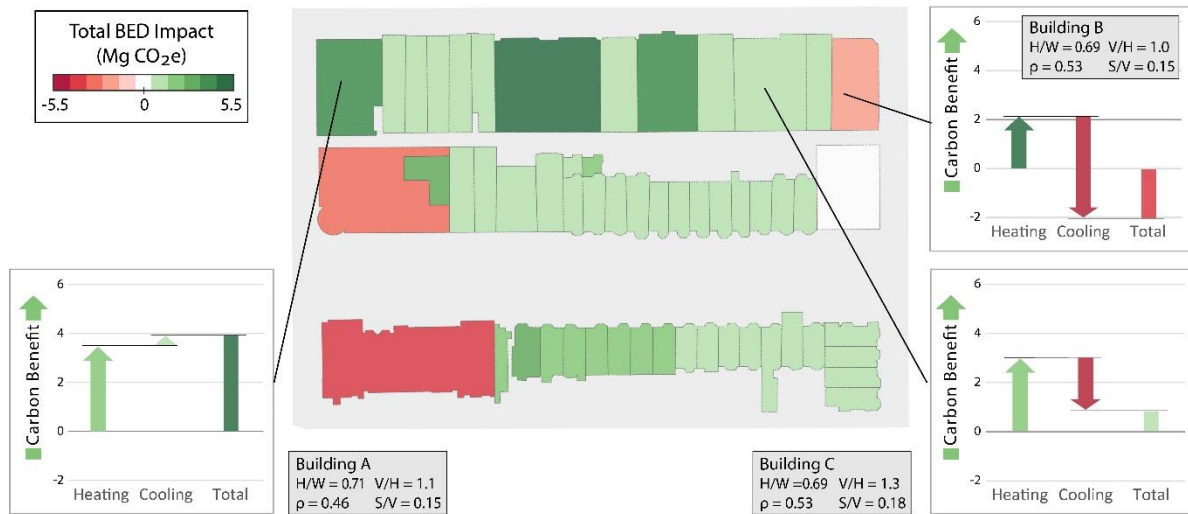
366 3.2 Citywide case study results and discussion

367 Each of the more than 100,000 buildings in Boston was evaluated to estimate the prevailing local
368 morphology including the canyon aspect ratio (H/W), shape factor (S/V), areal density (ρ_b) and
369 façade density (ρ_f). This information was used to assign each building a local climate zone based
370 on the characteristics of its neighborhood. Simulation-based meta-models were developed and
371 applied to predict changes in BED due to a 0.2 increase in pavement albedo for each of these
372 buildings for its LCZ neighborhood.

373 3.2.1 Building Level Results

374 Figure 6 shows the total 50-year GWP savings for a neighborhood of Boston at the individual
375 building level from increasing pavement albedo by 0.2. It is important to note that there are
376 limitations when directly applying meta-models at the individual building level. It is quite possible
377 that any given building result may be incorrect. However, because of the non-linear response
378 observed (see Figure 3 and Figure 4), aggregating such granular results should provide a useful
379 estimate of the GWP savings or burdens due to the increase in pavement albedo at the
380 neighborhood level. As is apparent from Figure 6, that results can vary significantly even for
381 buildings in close proximity. Three buildings, labeled as A, B, and C in Figure 6, highlight some
382 of these differences. All three buildings experience urban morphology conditions indicative of
383 LCZ 2. We see that building B experiences a cooling burden while building A experiences a
384 cooling benefit. Considering the trends displayed in Figures 3 and 4, this difference appears to
385 emerge due to a larger S/V and larger ρ_f but is moderated by a smaller ρ_b . All three buildings

386 experience a heating benefit due to albedo change, but the magnitude varies. Again, comparing A
 387 and B, we see that B has a lower heating benefit due primarily to a larger S/V and ρ_b . Similarly,
 388 comparing B and C, we see that B has a higher burden due to change in cooling and a lower benefit
 389 due to change in heating than C. Both of these effects are primarily driven by the slightly higher
 390 S/V for building C. The higher ρ_f for building C reinforces the cooling difference while
 391 simultaneously muting the difference in heating demand.



392

393 *Figure 6. GWP savings from BED at building level due to a 0.2 increase in pavement albedo in Boston*
 394 *over 50 years (a red hue indicates a GWP burden). All results are in terms of Mg CO₂eq for a 50-year*
 395 *analysis period.*
 396

397 3.2.2 Census tract level

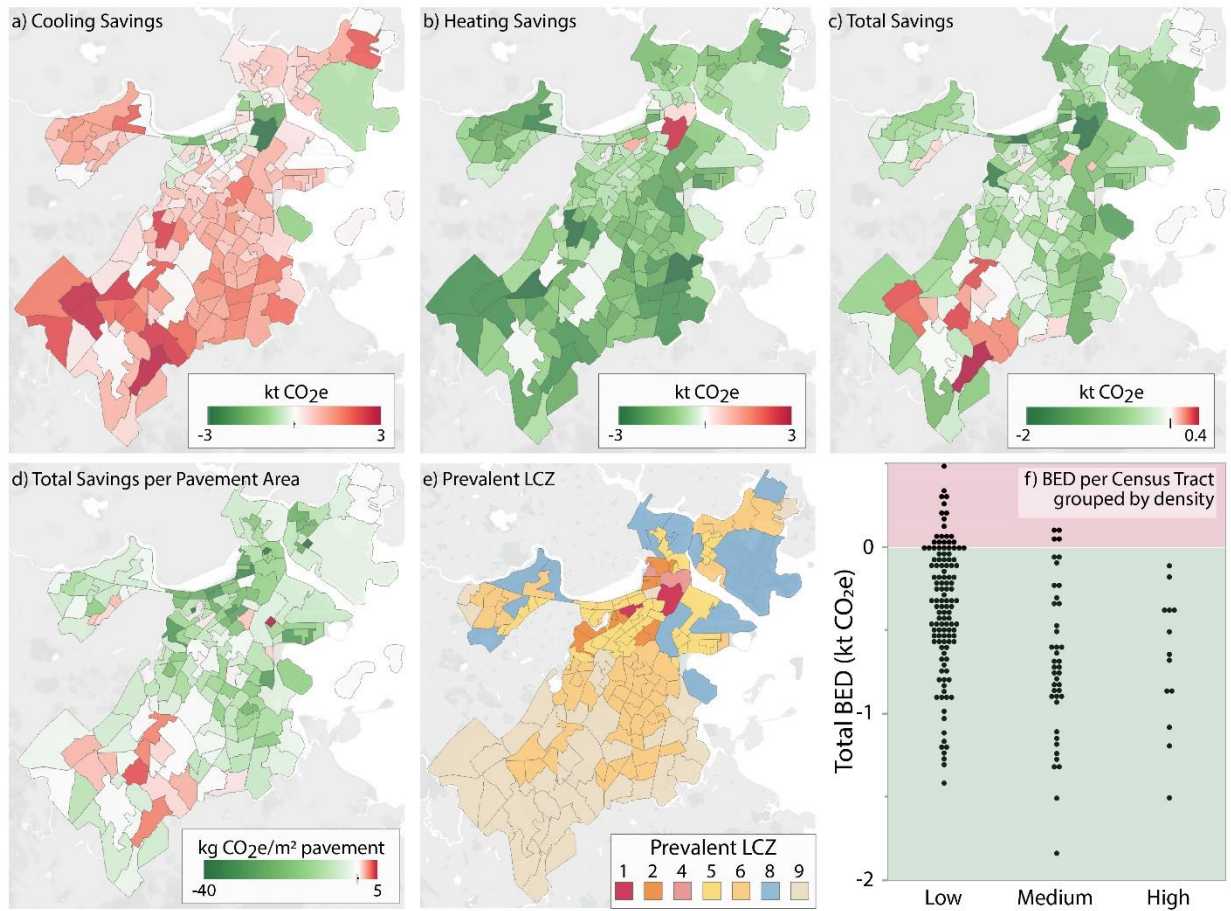
398 Changes in BED at the census tract (CT) level are aggregated by adding up the building-level
 399 results in each census tract. These aggregated results are likely more indicative of areas of high

400 potential for detailed study. The aggregated results for a 0.2 increase in pavement albedo are shown
401 in Figure 7. The BED impacts on cooling (Figure 7a), heating (Figure 7b), and the total of the two
402 (Figure 7c) are shown in the panels across the top row of Figure 7. From this figure, we see a broad
403 range of BED impacts ranging from an intense burden (dark red) to an intense saving (dark green).
404 It can be seen from the maps that increasing pavement albedo in Boston tends to increase cooling
405 burdens (see Figure 7a), but generally reduces heating burdens (see Figure 7b). Whether a
406 neighborhood experiences a net GHG benefit depends on the balance of these two effects. To help
407 explore this, Figure 7e shows the most prevalent LCZ for each census tract in Boston. Building
408 density generally decreases from LCZ 1 (compact high-rise – red color) to LCZ 9 (sparsely built
409 – tan color). Generally, we see that neighborhoods are more likely to experience a net benefit when
410 their density is high (LCZs 1-4) than when they are low (LCZs 8 or 9). This pattern of behavior is
411 shown more quantitatively in Figure 7f. In this plot each dot represents the total BED result for
412 one CT. This is the same data that is used to color Figure 7c. CTs are grouped as high density
413 (average density greater than 0.35), medium ($0.35 \geq \rho_b \geq 0.25$), and low ($\rho_b < 0.25$). Of the 14
414 high-density LCZs, zero (0) show a net impact. For the 42 medium density CTs, four (4) or 10%
415 show a net impact. Finally, for 121 the low-density CTs, 15% (18) show a net negative impact.
416 Overall, model results indicate that 89% of the Boston CTs (157 out of 177 or 83% of land area)
417 would experience reduced GHG emissions from building energy demand if pavements in that CT
418 had a higher albedo. Within the city of Boston there are nearly 1,300 paved miles (2,080 km) of

419 road. These results suggest that raising the albedo of approximately 1,100 of those miles (1,770
420 km) would lead to carbon benefits of about 91,720 metric tons over the next fifty years.

421 Results from two additional scenarios are presented in the Supporting Information section S10.
422 One scenario considers the impact of emissions from the non-baseload grid [45]. The base-load
423 scenario considers the annual average hourly suppliers of energy that operate generally while non-
424 base load suppliers (short-term marginal technology) are those that supply the demand in peak
425 demand hours. For this case, the emission factors for non-baseload cooling and heating were
426 calculated as 0.732 and 0.352 kg CO₂eq/kWh, respectively. With this higher (than the baseload)
427 burden for cooling, we see GHG benefit for changing pavement albedo in only 55% of CTs (49%
428 of urban area). The second additional scenario considers the impact of the long-term marginal
429 generating technology [46]. Under these conditions, emissions factors for cooling and heating fall
430 to 0.309 and 0.303 kg CO₂eq/kWh, respectively, and GHG benefit is observed in all but one CT
431 (>99% of urban area).

432 The results shown in the Figure 7 maps make clear that the net effect of changing pavement albedo
433 depends on urban morphology. Ultimately, to make a final evaluation of the best alternative for
434 each neighborhood, this information will need to be combined with other data on the life cycle
435 impact of pavements. To that end, we also show the total BED impact per area of pavement
436 converted by census tract in Figure 7d. This result trends similarly to the aggregate total savings
437 (Figure 7c).



438

439 *Figure 7. GWP impacts due to a 0.2 increase in pavement albedo in Boston at census-tract level over a*
 440 *50-year analysis period (red indicates a GWP burden). Impacts due to changes in (a) cooling, (b)*
 441 *heating, and (c) total (i.e. sum of the two) are shown in top row of the figure. The total per area of*
 442 *pavement in the census tract is shown in (d). The prevailing LCZ in each census tract is shown in (e). (f)*
 443 *plots the same information as in (c), but census tracts are grouped by their relative density. Each dot*
 444 *represents on census tract (two highly positive points in the High-density group are not plotted to*
 445 *improve clarity of the other points.) Figures generated in Tableau software. Underlying map images and*
 446 *geographic data © Mapbox © OpenStreetMap.*
 447

448 Overall, the results presented here confirm the hypothesis that urban morphology plays a
 449 significant role in shaping the impact of pavement albedo modification on BED. Several

450 morphological parameters are identified as influential factors, including building density, canyon
451 aspect ratio, façade density, and building surface area to volume ratio. Results from the
452 experimental design and the case study of Boston demonstrate that local context can shift the
453 impact of albedo change from benefit to burden.

454 The Boston case analysis suggests that there are many neighborhoods in which an increase in
455 pavement albedo would create a carbon emissions benefit. Therefore, it is recommended that these
456 strategies be explored in more detail in those contexts, of course using tools that consider urban
457 morphology and microclimate. In addition, a more comprehensive evaluation of the impact of
458 reflective pavements is necessary, considering other phases and components in a pavement's life
459 cycle such as material extraction, construction, vehicle fuel consumption, and end-of-life. Further
460 research on the impact of building properties on BED as well as data collection on the evolution
461 of pavement albedo due to aging and resurfacing would improve the robustness of the model for
462 supporting sustainable pavement designs. Using multiple weather files within a city location will
463 give a more representative condition of the climate in this analysis, particularly for those regions
464 that are adjacent to bodies of water. Further research is required to generate zone-specific climate
465 data for such a high-resolution analysis.

466 **4 CONCLUSIONS**

467 This study proposes a high-resolution approach to quantify the global warming impact changes
468 attributed to cool pavements in an urban vicinity, using both a coupled physical-simulation model

469 and a machine-learning model. The approach was implemented in a case study of the City of
470 Boston to assess the net BED effects of cool pavements. Results from the building-level analysis
471 show that the net GHG saving of changing pavement albedo depends on urban morphology. In
472 addition, the census tract results demonstrate that increasing pavement albedo usually reduces
473 carbon emissions from BED for high and low-density neighborhoods, while results from medium-
474 density neighborhoods were mixed. In fact, increasing the albedo would lead to BED GHG
475 benefits in 88% of neighborhoods in Boston. In addition, the albedo increase would yield more
476 than 90,000 metric tons of reduced carbon emissions over the next fifty years in 1,770 km of urban
477 roads. One should note that the obtained results may not be generalized to other cities located in
478 different climate zones. In fact, in other cities, the heating and cooling degree days as well as urban
479 texture can possibly induce a completely different conclusion. Nevertheless, the proposed model
480 and its outcome open doors for an assessment of the albedo effect on building energy demand as
481 a means of supporting robust decisions on cool pavements while considering the heterogeneity
482 that exists within urban neighborhoods in any city.

483 ACKNOWLEDGMENTS

484 This research was conducted as part of the Concrete Sustainability Hub at the Massachusetts
485 Institute of Technology, which is supported by the Portland Cement Association and the Ready
486 Mixed Concrete Research and Education Foundation.

487 **5 REFERENCES**

- 488 [1] Pravin Bhiwapurkar, “Urban Microclimates and Energy Efficient Buildings,” in *Special*
489 *Issue: Future of Architectural Research/ARCC 2015 Conference*, 2015.
- 490 [2] L. Yang, F. Qian, D.-X. Song, and K.-J. Zheng, “Research on Urban Heat-Island Effect,”
491 *Procedia Eng.*, vol. 169, pp. 11–18, 2016.
- 492 [3] M. Santamouris, “Cooling the cities - A review of reflective and green roof mitigation
493 technologies to fight heat island and improve comfort in urban environments,” *Sol. Energy*,
494 vol. 103, pp. 682–703, 2014.
- 495 [4] A. H. Rosenfeld, H. Akbari, J. J. Romm, and M. Pomerantz, “Cool communities: strategies
496 for heat island mitigation and smog reduction,” *Energy Build.*, vol. 28, no. 1, pp. 51–62,
497 Aug. 1998.
- 498 [5] D. Li, E. Bou-Zeid, and M. Oppenheimer, “The effectiveness of cool and green roofs as
499 urban heat island mitigation strategies,” *Environ. Res. Lett.*, vol. 9, no. 5, p. 055002, 2014.
- 500 [6] H. Akbari, S. Menon, and A. Rosenfeld, “Global cooling: Increasing world-wide urban
501 albedos to offset CO₂,” *Clim. Change*, vol. 94, no. 3–4, pp. 275–286, 2009.
- 502 [7] Y. Han, J. E. Taylor, and A. L. Pisello, “Exploring mutual shading and mutual reflection
503 inter-building effects on building energy performance,” *Appl. Energy*, vol. 185, pp. 1556–
504 1564, Jan. 2017.
- 505 [8] A. J. Monaghan, L. Hu, N. A. Brunsell, M. Barlage, and O. V. Wilhelmli, “Evaluating the
506 impact of urban morphology configurations on the accuracy of urban canopy model
507 temperature simulations with MODIS,” *J. Geophys. Res. Atmos.*, vol. 119, no. 11, pp. 6376–
508 6392, Jun. 2014.
- 509 [9] Y. Kikegawa, Y. Genchi, H. Yoshikado, and H. Kondo, “Development of a numerical
510 simulation system toward comprehensive assessments of urban warming countermeasures
511 including their impacts upon the urban buildings’ energy-demands,” *Appl. Energy*, vol. 76,
512 no. 4, pp. 449–466, 2003.
- 513 [10] Y. Kikegawa, Y. Genchi, H. Kondo, and K. Hanaki, “Impacts of city-block-scale
514 countermeasures against urban heat-island phenomena upon a building’s energy-
515 consumption for air-conditioning,” *Appl. Energy*, vol. 83, no. 6, pp. 649–668, Jun. 2006.
- 516 [11] F. Salamanca, A. Krpo, A. Martilli, and A. Clappier, “A new building energy model coupled

- 517 with an urban canopy parameterization for urban climate simulations—part I. formulation,
518 verification, and sensitivity analysis of the model,” *Theor. Appl. Climatol.*, vol. 99, no. 3–
519 4, pp. 331–344, Jan. 2010.
- 520 [12] A. Krpo, F. Salamanca, A. Martilli, and A. Clappier, “On the Impact of Anthropogenic Heat
521 Fluxes on the Urban Boundary Layer: A Two-Dimensional Numerical Study,” *Boundary-
522 Layer Meteorol.*, vol. 136, no. 1, pp. 105–127, Jul. 2010.
- 523 [13] F. Salamanca *et al.*, “A Study of the Urban Boundary Layer Using Different Urban
524 Parameterizations and High-Resolution Urban Canopy Parameters with WRF,” *J. Appl.
525 Meteorol. Climatol.*, vol. 50, no. 5, pp. 1107–1128, May 2011.
- 526 [14] D. Mauree, S. Coccolo, J. Kaempf, and J.-L. Scartezzini, “Multi-scale modelling to evaluate
527 building energy consumption at the neighbourhood scale,” *PLoS One*, vol. 12, no. 9, p.
528 e0183437, Sep. 2017.
- 529 [15] S. J. Quan, A. Economou, T. Grasl, and P. P.-J. Yang, “Computing Energy Performance of
530 Building Density, Shape and Typology in Urban Context,” *Energy Procedia*, vol. 61, pp.
531 1602–1605, 2014.
- 532 [16] I. Muñoz, P. Campra, and A. R. Fernández-Alba, “Including CO₂-emission equivalence of
533 changes in land surface albedo in life cycle assessment. Methodology and case study on
534 greenhouse agriculture,” *Int. J. Life Cycle Assess.*, vol. 15, no. 7, pp. 672–681, Jun. 2010.
- 535 [17] F. Cherubini, R. M. Bright, and A. H. Strømman, “Site-specific global warming potentials
536 of biogenic CO₂ for bioenergy: contributions from carbon fluxes and albedo dynamics,”
537 *Environ. Res. Lett.*, vol. 7, no. 4, p. 045902, 2012.
- 538 [18] R. M. Bright, F. Cherubini, and A. H. Strømman, “Climate impacts of bioenergy: Inclusion
539 of carbon cycle and albedo dynamics in life cycle impact assessment,” *Environ. Impact
540 Assess. Rev.*, vol. 37, pp. 2–11, 2012.
- 541 [19] H. Cai, J. Wang, Y. Feng, M. Wang, Z. Qin, and J. B. Dunn, “Consideration of land use
542 change-induced surface albedo effects in life-cycle analysis of biofuels,” *Energy Environ.
543 Sci.*, vol. 9, no. 9, pp. 2855–2867, Aug. 2016.
- 544 [20] N. Yaghoobian, J. Kleissl, and E. S. Krayenhoff, “Modeling the Thermal Effects of
545 Artificial Turf on the Urban Environment,” *J. Appl. Meteorol. Climatol.*, vol. 49, no. 3, pp.
546 332–345, Mar. 2010.
- 547 [21] N. Yaghoobian and J. Kleissl, “Effect of reflective pavements on building energy use,”

- 548 *Urban Clim.*, vol. 2, pp. 25–42, Dec. 2012.
- 549 [22] H. Li, J. Harvey, and A. Kendall, “Field measurement of albedo for different land cover
550 materials and effects on thermal performance,” *Build. Environ.*, vol. 59, pp. 536–546, Jan.
551 2013.
- 552 [23] G. Vox, A. Maneta, and E. Schettini, “Evaluation of the radiometric properties of roofing
553 materials for livestock buildings and their effect on the surface temperature,” *Biosyst. Eng.*,
554 vol. 144, pp. 26–37, Apr. 2016.
- 555 [24] D. B. Crawley *et al.*, “EnergyPlus: Creating a new-generation building energy simulation
556 program,” *Energy Build.*, vol. 33, no. 4, pp. 319–331, 2001.
- 557 [25] H. E. Gilbert *et al.*, “Energy and environmental consequences of a cool pavement
558 campaign,” *Energy Build.*, vol. 157, pp. 53–77, 2017.
- 559 [26] D. Bachman, *Grasshopper: Visual Scripting for Rhinoceros 3D*. New York, NY, USA:
560 Industrial Press, Inc., 2017.
- 561 [27] A. S. Mostapha Sadeghipour Roudsari, Michelle Pak, “Ladybug: a parametric
562 environmental plugin for grasshopper to help designers create an environmentally-
563 conscious design,” in *Proceedings of the 13th international IBPSA conference*, 2013, pp.
564 3128–3135.
- 565 [28] B. Bueno, L. Norford, J. Hidalgo, and G. Pigeon, “The urban weather generator,” *J. Build.*
566 *Perform. Simul.*, vol. 6, no. February 2015, pp. 1–13, Jul. 2012.
- 567 [29] I. D. Stewart and T. R. Oke, “Local Climate Zones for Urban Temperature Studies,” *Bull.*
568 *Am. Meteorol. Soc.*, vol. 93, no. 12, pp. 1879–1900, Dec. 2012.
- 569 [30] American Concrete Pavement Association, *Albedo: A Measure of Pavement Surface*
570 *Reflectance*. Skokie, IL: American Concrete Pavement Association (ACPA), 2002.
- 571 [31] Robert McNeel & Associates, “Rhinoceros,” 2019. [Online]. Available: www.rhino3d.com.
- 572 [32] A. Nakano, B. Bueno, L. Norford, and C. F. Reinhart, “Urban Weather Generator-A novel
573 workflow for integrating urban heat island effect within urban design process,” in
574 *Proceedings of BS2015: 14th Conference of International Building Performance*
575 *Simulation Association*, 2015, pp. 1901–1908.
- 576 [33] B. Bueno, M. Roth, L. Norford, and R. Li, “Computationally efficient prediction of canopy

- 577 level urban air temperature at the neighbourhood scale,” *Urban Clim.*, vol. 9, pp. 35–53,
578 Sep. 2014.
- 579 [34] DOE Building Energy Codes Program, “ANSI/ASHRAE/IES Standard 90.1-2010 |
580 Building Energy Codes Program,” 2011. .
- 581 [35] H. Azarijafari, A. Yahia, and M. Ben Amor, “Life cycle assessment of pavements:
582 Reviewing research challenges and opportunities,” *J. Clean. Prod.*, vol. 112, 2016.
- 583 [36] H. Li, C. Author, J. Harvey, Y. He, and P. Li, “Pavement Treatment Practices and Dynamic
584 Albedo Change of Urban Pavement Network in California,” 2014.
- 585 [37] X. Liu, Q. Cui, and C. Schwartz, “Greenhouse gas emissions of alternative pavement
586 designs: framework development and illustrative application.,” *J. Environ. Manage.*, vol.
587 132, pp. 313–22, Jan. 2014.
- 588 [38] P. J. Rosado and R. Levinson, “Potential benefits of cool walls on residential and
589 commercial buildings across California and the United States: Conserving energy, saving
590 money, and reducing emission of greenhouse gases and air pollutants,” *Energy Build.*, Sep.
591 2019.
- 592 [39] D. S. Rui Guo, Yafeng Gao, Chaoqun Zhuang, Per Heiselberg, Ronnen Levinson, Xia Zhao,
593 “Optimization of cool roof and night ventilation in office buildings: A case study in Xiamen,
594 China,” *Renew. Energy*, vol. 147, pp. 2279–2294, 2020.
- 595 [40] Commonwealth of Massachusetts Executive Office of Energy and Environmental Affairs,
596 “Office of Geographic Information (Mass GIS),” 2008. [Online]. Available:
597 <http://www.mass.gov/mgis/>.
- 598 [41] US Census Bureau, “TIGER/Line® Shapefiles and TIGER/Line® Files,” 2019. [Online].
599 Available: <https://www.census.gov/programs-surveys/geography.html>.
- 600 [42] B. Behsh, “Building form as an option for enhancing the indoor thermal conditions,” in
601 *Building Physics 2002 - 6th Nordic Symposium*, 2002, vol. 18, pp. 759–766.
- 602 [43] QGIS Development Team, “QGIS geographic information system,” *Open Source*
603 *Geospatial Foundation Project*, 2009. [Online]. Available: <http://qgis.osgeo.org>.
- 604 [44] M. Moradi *et al.*, “The Vertical City Weather Generator (VCWG v1.0.0),” *Geosci. Model*
605 *Dev. Discuss.*, pp. 1–42, Aug. 2019.

- 606 [45] U.S. EIA, “State Profile and Energy Estimates Massachusetts Profile,” 2018. [Online].
607 Available: <https://www.eia.gov/state/?sid=MA>.
- 608 [46] L. Vandepaer, K. Treyer, C. Mutel, C. Bauer, and B. Amor, “The integration of long-term
609 marginal electricity supply mixes in the ecoinvent consequential database version 3.4 and
610 examination of modeling choices,” *Int. J. Life Cycle Assess.*, vol. 24, no. 8, pp. 1409–1428,
611 Aug. 2019.
- 612
- 613